Impaired structural and reserved functional topological organizations of brain networks in Parkinson's disease with freezing of gait

Lina Wang[1#], Caiting Gan[1#], Huimin Sun[1#], Min Ji[1], Heng Zhang[1], Xingyue Cao[1], Min Wang[2], Yongsheng Yuan[1], Kezhong Zhang[1]

[1]Department of Neurology, The First Affiliated Hospital of Nanjing Medical University, Nanjing, China; [2]Department of Radiology, The First Affiliated Hospital of Nanjing Medical University, Nanjing, China

Contributions: (I) Conception and design: L Wang, C Gan, H Sun, K Zhang; (II) Administrative support: K Zhang; (III) Provision of study materials or patients: None; (IV) Collection and assembly of data: M Ji, H Zhang, X Cao, M Wang, Y Yuan; (V) Data analysis and interpretation: L Wang, C Gan, H Sun, K Zhang; (VI) Manuscript writing: All authors; (VII) Final approval of manuscript: All authors.

[#]These authors contributed equally to this work.

Correspondence to: Kezhong Zhang. Department of Neurology, The First Affiliated Hospital of Nanjing Medical University, 300 Guangzhou Road, Nanjing 210029, China. Email: kezhong_zhang1969@126.com.

Background: Freezing of gait (FOG) is a common disabling motor disturbance in Parkinson's disease (PD). Our study aimed to probe the topological organizations of structural and functional brain networks and their coupling in FOG.

Methods: In this cross-sectional retrospective study, a total of 30 PD patients with FOG (PD-FOG), 40 patients without FOG, and 25 healthy controls (HCs) underwent clinical assessments and magnetic resonance imaging (MRI) scanning. Large-scale structural and functional brain networks were constructed. Subsequently, global and nodal graph theoretical properties and functional-structural coupling were investigated. Finally, correlations between the altered brain topological properties and freezing severity were analyzed in PD-FOG.

Results: For structural networks, at the global level, PD-FOG exhibited increased normalized characteristic path length (P=0.040, Bonferroni-corrected) and decreased global efficiency (P=0.005, Bonferroni-corrected) compared with controls, and showed reduced global (P=0.001, Bonferroni-corrected) and local (P=0.032, Bonferroni-corrected) efficiency relative to patients without FOG. At the nodal level, nodal efficiency of structural networks was reduced in PD-FOG compared with PD patients without FOG, located in the left supplementary motor area (SMA), gyrus rectus, and middle cingulate cortex (MCC) (all P<0.05, Bonferroni-corrected). Notably, altered global and nodal properties of structural networks were significantly correlated with Freezing of Gait Questionnaire scores [all P<0.05, false discovery rate (FDR)-corrected]. However, only an increase in local efficiency (P=0.003, Bonferroni-corrected) of functional networks was identified in PD-FOG compared with those without FOG. No significant structural-functional coupling was detected among the 3 groups.

Conclusions: This study demonstrates the extensively impaired structural and relatively reserved functional network topological organizations in PD-FOG. Our results also provide evidence that the pathogenesis of PD-FOG is primarily attributable to network vulnerability established by crucial structural damage, especially in the left SMA, gyrus rectus, and MCC.

Keywords: Freezing of gait (FOG); Parkinson's disease (PD); topology; structural-functional coupling; supplementary motor area (SMA)

Introduction

Patients with advanced Parkinson's disease (PD) often manifest freezing of gait (FOG), a gait disorder characterized by a brief and sudden inability to take a step despite an intention to walk (1). As a paroxysmal phenomenon, FOG is often induced by specific triggers and usually occurs during gait initiation, turning, and dual-task walking. Despite that FOG increases the risk of falls, affects mobility, and even reduces quality of life (2), there are few effective treatments that can reliably alleviate FOG (3). Although the pathophysiological mechanisms underpinning FOG in PD are still unclear, advanced neuroimaging studies have gained relevant insights into the pathophysiology of FOG in PD (4).

Growing magnetic resonance imaging (MRI) studies have demonstrated structural and functional abnormalities in multiple cortical and subcortical brain regions in PD patients with FOG (PD-FOG). Damage to the mesencephalic locomotor region (MLR), especially the pedunculopontine nucleus (PPN), could lead to cortical and striatal cholinergic denervation (5) or a paroxysmal inhibition secondary to altered basal ganglia inputs (6), ultimately resulting in FOG. Cerebellar gray matter (GM) loss and white matter (WM) tract changes (7,8), as well as altered functional connectivity with the frontal cortex (9) have been shown to affect gait planning and execution in PD-FOG. Regarding the vital role of the basal ganglia in PD-FOG, the most accepted hypotheses include the "interference model", suggesting that FOG might result from convergence dysfunction and overload of segregate basal ganglia circuits, such as the oculomotor, sensorimotor, associative, and limbic loops (10,11). In addition to subcortical damage, altered frontoparietal networks responsible for attention, executive, and visuospatial functions have also been implicated in the pathophysiological mechanisms of PD-FOG (12-14). Lastly, the limbic system including the amygdala is also involved in the development of FOG in PD (15). Thus, compelling evidence indicates that FOG is a complex network disorder involving motor, cognitive, and limbic networks, which implicates various cortical and subcortical brain regions in PD (16-18).

Recently, advances in graph-based network theory have allowed direct, noninvasive characterization of brain network topological organizations in multiple diseases (19,20). Complex human brain networks are typical small-world organizations, with an optimal balance between global integration and local segregation (21). With this approach, we elucidated impaired WM topological properties in PD patients with levodopa-induced dyskinesias (22). Previously, several studies have illustrated topological changes in structural or functional systems in PD-FOG (12,23-25). Using diffusion tensor imaging (DTI), Hall *et al.* confirmed FOG-related structural integration and modularity alterations within the frontal and parietal cortices (23). With resting-state functional MRI (rs-fMRI) temporal correlations, Maidan *et al.* validated altered organization of the dorsal attention network in PD-FOG (12). Two other studies have suggested that FOG in PD is also associated with sensorimotor, frontoparietal, and visual network dysfunctions (24,25). Recently, a longitudinal study demonstrated that disrupted regional topological organization might contribute to the development of FOG in PD (26). Hence, previous topological studies have deepened our understanding of the neural mechanisms underlying PD-FOG. However, these studies only focused on a single structural or functional system and could not identify which systems play a major role in the pathogenesis of FOG in PD. Meanwhile, they also ignored the coupling patterns between structural and functional networks, which might provide novel insights into the reconfiguration of PD-FOG neural networks (27). Therefore, in the present study, we first aimed to systematically investigate the alterations of large-scale structural and functional brain networks and their coupling patterns in PD-FOG. We present the following article in accordance with the Strengthening the Reporting of Observational Studies in Epidemiology (STROBE) reporting checklist (available at https://qims.amegroups.com/article/view/10.21037/qims-22-351/rc).

Methods

Participants

This was a cross-sectional retrospective study. Cases were consecutively recruited from March 2017 to November 2019 in the Department of Neurology, the First Affiliated
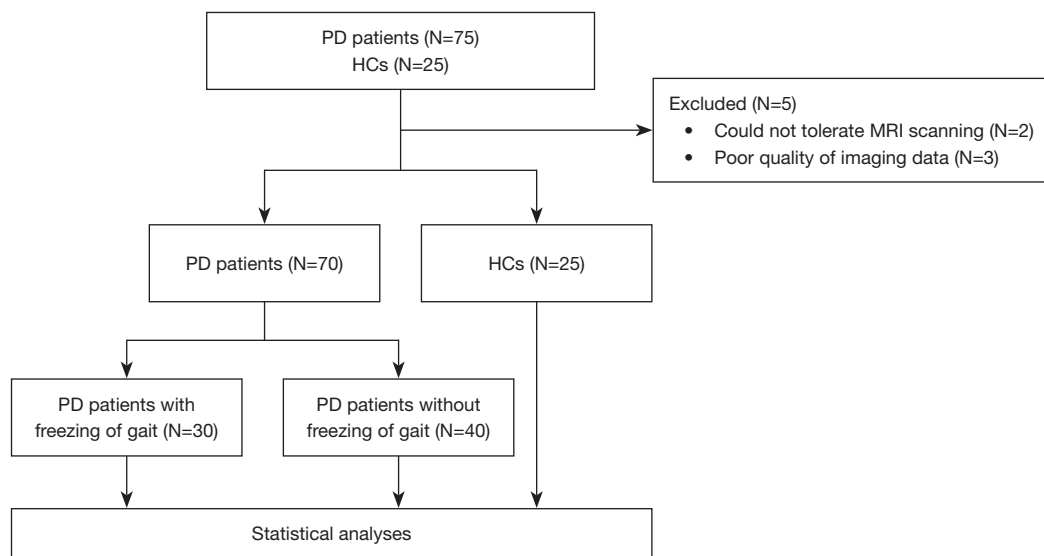
Figure 1 Study flow diagram. PD, Parkinson's disease; HCs, healthy controls; N, numbers.

Hospital of Nanjing Medical University. A total of 75 patients meeting the diagnosis of PD according to the clinical criteria of the Movement Disorder Society (28) were enrolled in the study. Additionally, they had no (I) family history of PD; (II) contraindications of MRI scans; (III) focal brain lesions; (IV) global cognitive impairment [Mini-Mental State Examination (MMSE) score <24] (29); (V) intake of sedative and hypnotic medications; and (VI) other disorders interfering with gait, such as primary progressive freezing gait, normal pressure hydrocephalus, and vascular parkinsonism. Two PD patients withdrew from the study because they could not tolerate MRI scanning. Three patients were excluded due to the poor quality of imaging data. Finally, 70 PD patients were enrolled in our study. Among these patients, we ascertained FOG individuals based on a score of 1 or above on item 3 of the FOG Questionnaire (FOG-Q) (30) and clinical freezing episodes observed by 2 researchers (K Zhang and L Wang) during 10 meter walking, turning, or moving through a narrow doorway. Considering the possible confounding effects of FOG subtypes, our study included only those FOG patients who experienced FOG both in drug OFF and ON states, namely, levodopa-resistant FOG (11). Finally, all PD patients were divided into PD-FOG (n=30) and PD patients without FOG (PD-nFOG, n=40) subgroups.

During the OFF state of drug withdrawal for 12 hours, all patients underwent an array of standardized clinical evaluations prior to MRI scanning (M Ji and H Zhang). Motor and FOG-related function was evaluated using the

Hoehn and Yahr (H&Y) stage (31), symptom-dominant side, part III of the Unified Parkinson's Disease Rating Scale (UPDRS-III) (32), the Tinetti Mobility Test (TMT) (33), the Timed Up and Go (TUG) test (34), and the FOG-Q. The Hamilton Anxiety Rating Scale (HAMA) (35) and the 24-item Hamilton Rating Scale for Depression (HAMD-24) (36) were applied to assess emotional state. The MMSE and Frontal Assessment Battery (FAB) (37) were used to assess global cognition and executive function. Lastly, total levodopa equivalent daily dose (LEDD) for each patient was calculated to describe the anti-parkinsonism medications administered (38).

The MRI scans were conducted at least 12 hours after withdrawal from drugs for all PD participants. According to the study size of previous imaging studies (22), 25 age-, gender-, and education level-matched healthy controls (HCs) participated in the study. None of the HCs had a family history of PD, cognitive impairment, or other neuropsychiatric diseases. The flow diagram is shown in *Figure 1*. The study was conducted in accordance with the Declaration of Helsinki (as revised in 2013) and was approved by the Ethical Committee of the First Affiliated Hospital of Nanjing Medical University. All participants gave written informed consent.

MRI data acquisition and preprocessing

All brain MRIs were performed on a 3.0 T Siemens MAGNETOM Verio whole-body MRI scanner (Siemens

Medical Solutions, Erlangen, Germany) equipped with eight-channel phase-array head coils. Tight foam and earplugs were used to fix the head and reduce noise. T1-weighted anatomical images, DTI, and rs-fMRI data were obtained for each participant. The DTI data were preprocessed using the Pipeline for Analyzing braiN Diffusion imAges (PANDA; https://www.nitrc.org/projects/panda/) with the following steps: brain extraction, realignment, eddy and motion artifact correction, diffusion tensor matrices calculation, and diffusion tensor tractography. The rs-fMRI data preprocessing was performed using Data Processing Assistant for rs-fMRI (DPARSF). Specific steps included the removal of the first 10 time points, slice timing, correction, realignment, spatial normalization, nuisance signal regression, smoothing, and band-pass filtering. Detailed scanning parameters and preprocessing steps are in Supplementary methods (Appendix 1).

Construction and calculation of brain networks

Nodes of structural and functional networks were defined based on an Anatomical Automatic Labeling (AAL) algorithm (including the cerebellum). Structural networks were constructed using DTI tractography, and functional networks were connected with rs-fMRI temporal series correlations. As a result, individual symmetric 116×116 structural and functional connectivity matrices were obtained. See Supplementary methods (Appendix 1) for detailed construction steps.

Topological properties of structural and functional networks at global and nodal levels were investigated with the GRaph thEoreTical Network Analysis (GRETNA; https://www.nitrc.org/projects/gretna/node). Before calculating the metrics, the following parameters were determined. First, as for 'sign of matrix', although previous rs-fMRI studies have shown that certain functional systems are anti-correlated (i.e., have a negative correlation) in their spontaneous brain activity, negative correlations may also be introduced by global signal removal, a preprocessing step that is currently controversial. Moreover, negative correlations may have detrimental effects on test-retest reliability and exhibit organizations different from positive correlations. Due to the above reasons, we chose only positive correlations in this study. Second, a thresholding procedure is typically applied to exclude the confounding effects of spurious relationships in interregional connectivity matrices. In this study, the 'value

of matrix element' method was used for structural network matrices, and 'network sparsity' was applied for functional network matrices. To reduce the signal-to-noise ratio and fake connections, interconnections between structural brain nodes were considered to exist if the number of interconnected WM fibers was >10 (22). Meanwhile, a threshold range of $0.05<S<0.40$ with an interval of 0.01 was set for functional networks. Then, the area under the curve (AUC) over the sparsity was further calculated for each functional matrix, providing a summarized scale for the topological characterization of brain networks independent of a single threshold selection. Thus, this approach enabled the exploration of between-group differences in relative network organization, which is sensitive to topological alterations in brain disorders (39).

In this study, 2 typical types of global metrics were explored: (I) small-world parameters, including normalized clustering coefficient (γ), normalized characteristic path length (λ), and small-worldness (σ); and (II) network efficiency parameters, including global efficiency (Eg) and local efficiency (Eloc). At the nodal level, nodal efficiency (Ne) and nodal local efficiency (NLe) of structural and functional networks were calculated.

Structural-functional coupling

Considered as network coupling value, Pearson correlation coefficients between structural and functional network matrices were documented for each participant (27). The calculation steps are detailed in Supplementary methods (Appendix 1).

Statistical analysis

Data were firstly inspected for normality using histograms and the Shapiro-Wilk test. Then, demographic and clinical characteristics of the 3 groups were compared by the chi-square test, one-way analysis of variance (ANOVA), Kruskal-Wallis test, or Mann-Whitney test, as appropriate. A P value <0.05 was set as significant. These analyses were conducted with SPSS 20.0 software (IBM Corp., Armonk, NY, USA).

Inter-group differences of global and nodal properties and structural-functional coupling were firstly analyzed by one-way analyses of covariance (ANCOVAs), adjusted for age, gender, and education level. In particular, P<0.05 was considered significant for global parameters and structural-functional coupling, and P<0.05 corrected by Bonferroni

70

Wang et al. Topological brain organizations of FOG

Table 1 Demographic and clinical characteristics of all participants

Variables	PD-FOG (n=30)	PD-nFOG (n=40)	HCs (n=25)	P value
Demographic factors				
Gender (M/F)	17/13	25/15	17/8	0.688[a]
Age (y)	62.27±9.12	61.80±7.81	60.36±7.86	0.678[b]
Education (y)	9.73±4.41	11.25±2.92	11.36±3.75	0.240[c]
Clinical variables				
Disease duration (y)	6.32±3.32	6.37±4.77	NA	0.608[d]
H&Y stage	2.40±0.52	2.24±0.49	NA	0.175[d]
LEDD (mg/d)	645.26±265.88	686.53±383.43	NA	0.533[d]
UPDRS-III	33.53±9.76	29.75±14.88	NA	0.075[d]
Symptom-dominant side (L/R/B)	11/11/8	21/14/5	NA	0.246[a]
HAMA	12.87±6.82	9.90±7.25	2.68±2.75	<0.001[c,*]
HAMD-24	12.43±8.02	8.50±7.22	2.08±2.43	<0.001[c,*]
MMSE	28.00±1.68	28.00±1.68	28.56±1.47	0.361[c]
FAB	15.43±2.47	15.70±2.31	16.60±1.41	0.226[c]
Gait-related characteristics				
Total TMT	18.30±7.11	23.43±6.11	NA	<0.001[d,*]
TMT balance subscale	11.10±4.21	13.73±3.76	NA	<0.001[d,*]
TMT gait subscale	7.20±3.45	9.70±2.89	NA	0.002[d,*]
TUG (s)	14.42±6.28	11.78±5.48	NA	0.034[d,*]
FOG-Q	12.70±5.61	NA	NA	NA

Data are presented as number or mean ± SD. *, P<0.05 was set as significant; [a], Chi-square test; [b], one-way analysis of variance; [c], Kruskal-Wallis test; [d], Mann-Whitney test. PD-FOG, Parkinson's disease patients with freezing of gait; PD-nFOG, Parkinson's disease patients without freezing of gait; HCs, healthy controls; M, male; F, female; y, year; H&Y stage, Hoehn and Yahr stage; LEDD, levodopa equivalent daily dose; UPDRS, Unified Parkinson's Disease Rating Scale; L, left; R, right; B, bilateral; HAMA, Hamilton Anxiety Rating Scale; HAMD-24, 24-item Hamilton Rating Scale for Depression; MMSE, Mini-Mental State Examination; FAB, Frontal Assessment Battery; TMT, Tinetti Mobility Test; TUG, Timed Up and Go; FOG-Q, Freezing of Gait Questionnaire; NA, not applicable; SD, standard deviation.

was considered significant for nodal parameters due to multiple comparisons. Once significant differences were detected in global, coupling, or nodal properties using one-way ANCOVAs, we performed the multiple comparison procedure (Bonferroni correction) for further between-group differences. All above graph theoretical analyses were performed with the statistical model of GRETNA.

To investigate the relationships between the altered brain network connectome and FOG severity, Pearson correlations were performed between altered brain topological properties and FOG-Q results in PD-FOG. False discovery rate (FDR) correction was subsequently applied due to multiple testing.

Results

Demographics and clinical data

The demographic and clinical characteristics of 95 participants are presented in *Table 1*. No significant differences in gender, age, education level, and cognitive and executive function were observed among the 3 groups. The PD-FOG and PD-nFOG showed similar disease duration, H&Y stage, symptom-dominant side, LEDD, and UPDRS-III scores. However, PD-FOG exhibited a worse TMT, TUG, and FOG-Q performance compared with PD-nFOG. Notably, the HAMA and HAMD-24 scores were higher in PD-FOG and PD-nFOG relative to HCs. Therefore,

Table 2 Brain network global graph measures of all participants

Graph measures	PD-FOG	PD-nFOG	HCs	F value	P value	*Post hoc* (Bonferroni correction) analyses
Structural networks						
γ	6.389±0.731	5.995±0.827	5.790±0.676	2.942	0.058	
λ	1.235±0.078	1.209±0.052	1.194±0.044	3.406	0.038*	PD-FOG > HCs (P=0.040)
σ	5.180±0.552	4.956±0.621	4.852±0.548	1.104	0.336	
Eg	0.247±0.032	0.271±0.019	0.275±0.027	7.728	0.001*	PD-FOG < HCs (P=0.005); PD-FOG < PD-nFOG (P=0.001)
Eloc	0.379±0.064	0.418±0.043	0.409±0.044	3.560	0.033*	PD-FOG < PD-nFOG (P=0.032)
Functional networks						
γ	0.665±0.108	0.610±0.099	0.657±0.129	2.711	0.072	
λ	0.388±0.011	0.389±0.009	0.392±0.010	1.066	0.349	
σ	0.587±0.096	0.541±0.093	0.573±0.113	2.313	0.105	
Eg	0.183±0.007	0.182±0.009	0.180±0.007	0.633	0.533	
Eloc	0.261±0.006	0.255±0.007	0.260±0.008	5.961	0.004*	PD-FOG > PD-nFOG (P=0.003)
Structural-functional coupling						
Coupling	0.186±0.045	0.206±0.040	0.203±0.042	2.055	0.134	

Data are presented as mean ± SD. *, P<0.05 was set as significant. One-way ANCOVAs were applied to compare group differences in global properties and coupling among the 3 groups with age, gender, education level, and HAMA and HAMD-24 scores as covariances. *Post hoc* analyses (corrected by Bonferroni) were then used for between-group differences. PD-FOG, Parkinson's disease patients with freezing of gait; PD-nFOG, Parkinson's disease patients without freezing of gait; HCs, healthy controls; γ, normalized clustering coefficient; λ, normalized characteristic path length; σ, small-worldness; Eg, global efficiency; Eloc, local efficiency; ANCOVAs, analyses of covariance; HAMA, Hamilton Anxiety Rating Scale; HAMD-24, 24-item Hamilton Rating Scale for Depression; SD, standard deviation.

HAMA and HAMD-24 scores were included as covariates in subsequent imaging analyses in addition to age, gender, and education level to reduce potential confounding effects.

Structural and functional network topology analyses

Global parameters

Small-world organizations of structural and functional networks were confirmed in PD-FOG, PD-nFOG, and HCs. *Table 2* reveals significant differences in λ (F=3.406, P=0.038), Eg (F=7.728, P=0.001), and Eloc (F=3.560, P=0.033) of structural networks, and in Eloc (F=5.961, P=0.004) of functional networks using one-way ANCOVAs, adjusted for age, gender, education level, and HAMA and HAMD-24 scores. Specifically, for structural networks, PD-FOG showed increased λ (P=0.040, Bonferroni-corrected) and decreased Eg (P=0.005, Bonferroni-corrected) relative to HCs, and exhibited reduced Eg

(P=0.001, Bonferroni-corrected) and Eloc (P=0.032, Bonferroni-corrected) compared with PD-nFOG (*Figure 2A*). For functional networks, PD-FOG had increased Eloc (P=0.003, Bonferroni-corrected) compared to PD-nFOG (*Figure 2B*).

Structural-functional coupling

No significant structural-functional coupling was identified among all 3 groups.

Nodal parameters

At the nodal level, significant differences were observed in Ne (P<0.05, Bonferroni corrected) of structural networks among the 3 groups, after controlling for age, gender, education level, and HAMA and HAMD-24 scores (*Table 3*). Specifically, Ne of the left supplementary motor area (SMA), gyrus rectus, and middle cingulate cortex (MCC) was decreased in PD-FOG compared with PD-nFOG (*Figure 3*).
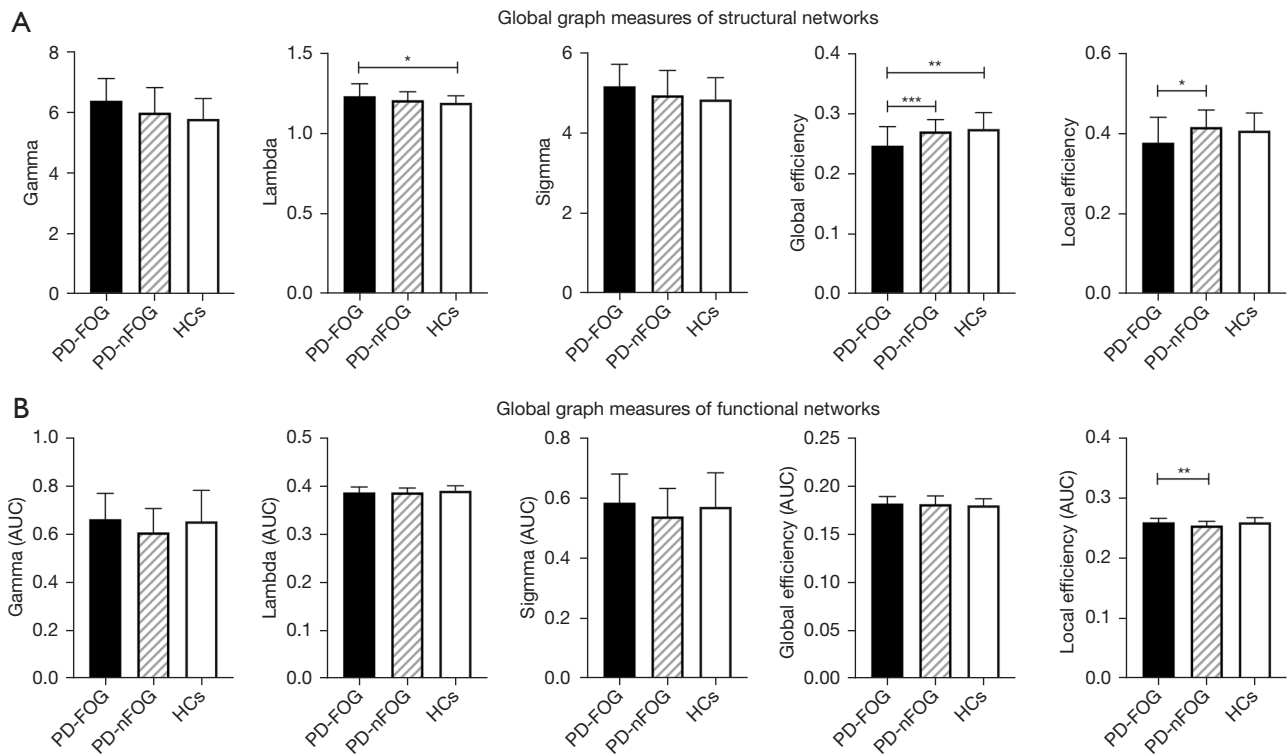
Figure 2 Global graph analyses of structural and functional networks. (A) For structural networks, increased lambda and decreased global efficiency were detected in PD-FOG compared with HCs, while decreased global and local efficiency were found in PD-FOG compared with PD-nFOG. (B) For functional networks, increased local efficiency (AUC) was identified in PD-FOG compared with PD-nFOG. *, $P<0.05$; **, $P<0.01$; ***, $P<0.001$. *Post hoc* P values for between-group comparisons were corrected by the Bonferroni method. PD-FOG, Parkinson's disease patients with freezing of gait; PD-nFOG, Parkinson's disease patients without freezing of gait; HCs, healthy controls; AUC, area under the curve.

Table 3 Brain network nodal properties in all participants

Brain regions (AAL)	Nodal efficiency of structural networks			F value	P value
	PD-FOG	PD-nFOG	HCs		
SMA.L	0.327±0.037	0.366±0.032	0.367±0.031	12.130	0.002
Rectus.L	0.251±0.041	0.295±0.028	0.294±0.037	10.929	0.005
MCC.L	0.308±0.034	0.336±0.025	0.338±0.032	8.570	0.039

Data are presented as mean ± SD. One-way ANCOVAs were used to explore nodal parameters of structural and functional networks among the 3 groups, adjusted for age, gender, education level, and HAMA and HAMD-24 scores. $P<0.05$ was considered significant after Bonferroni correction. AAL, anatomical automatic labeling; PD-FOG, Parkinson's disease patients with freezing of gait; PD-nFOG, Parkinson's disease patients without freezing of gait; HCs, healthy controls; L, left; SMA, supplementary motor area; MCC, middle cingulate cortex; SD, standard deviation; ANCOVAs, analyses of covariance.

Correlation analyses

For global measures of structural networks, negative correlations between Eg and FOG-Q ($r=-0.461$, $P_{FDR-corr}=0.024$) and Eloc and FOG-Q ($r=-0.419$, $P_{FDR-corr}=0.030$) were detected in PD-

FOG (*Figure 4A*). These results indicate that disrupted global properties in structural networks play an important role in the development of FOG. However, no correlations between global measures of functional networks and FOG-Q were
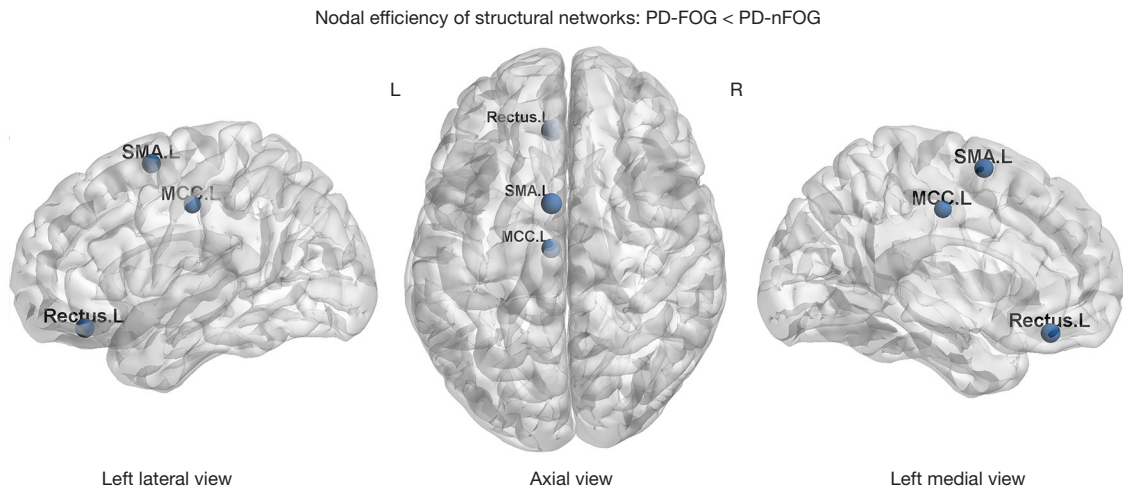
Nodal efficiency of structural networks: PD-FOG < PD-nFOG

Left lateral view   Axial view   Left medial view

Figure 3 Nodal graph analyses of structural and functional networks. For structural networks, PD-FOG showed reduced nodal efficiency in the left SMA, gyrus rectus, and MCC compared with PD-nFOG. The size of the dots indicated the relative T values from the two-sample *t*-test. PD-FOG, Parkinson's disease patients with freezing of gait; PD-nFOG, Parkinson's disease patients without freezing of gait; L, left; R, right; SMA, supplementary motor area; MCC, middle cingulate cortex.
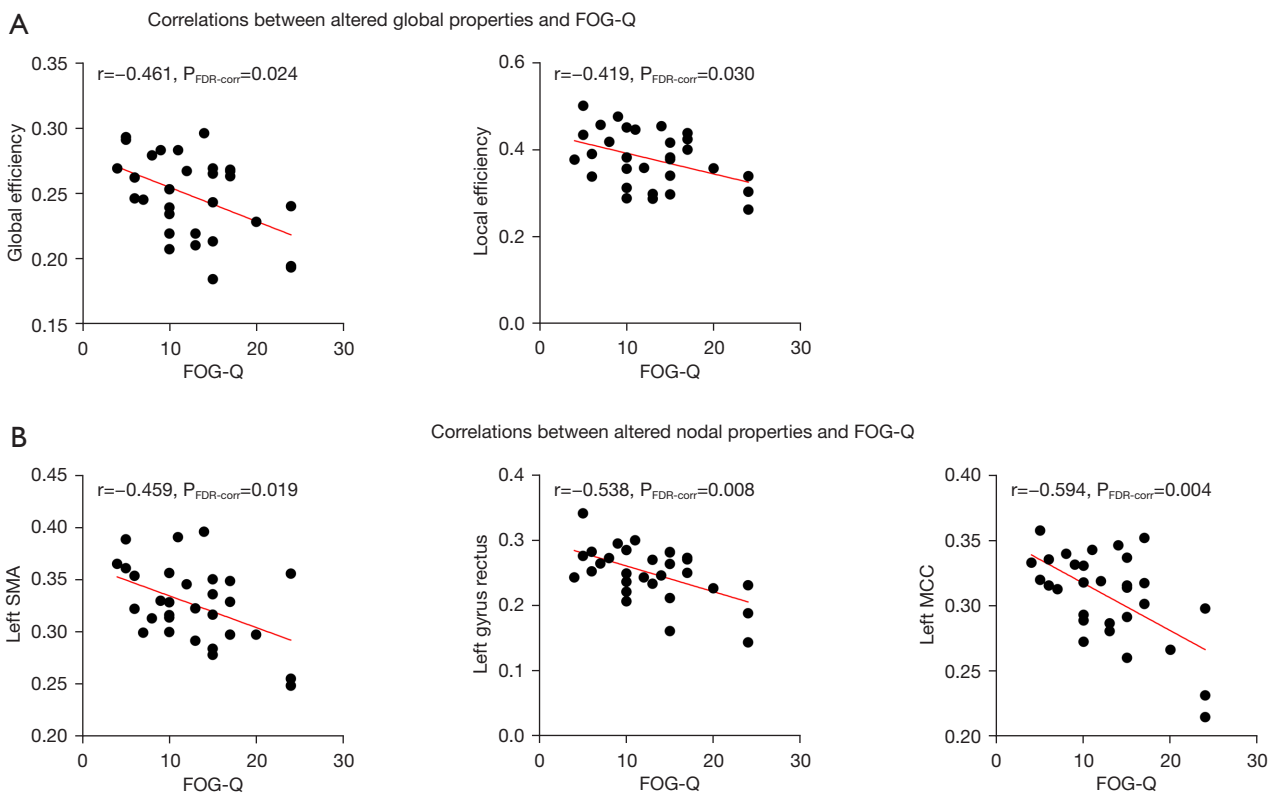

Figure 4 Correlation analyses between altered topological properties and FOG-Q. (A) At the global level, altered global and local efficiency of structural networks was negatively correlated with FOG-Q scores in PD-FOG. (B) At the nodal level, nodal efficiency of the left SMA, gyrus rectus, and MCC was negatively correlated with FOG-Q scores in PD-FOG. Correlation analyses were corrected by FDR. FOG-Q, Freezing of Gait Questionnaire; SMA, supplementary motor area; MCC, middle cingulate cortex; FDR, false discovery rate; PD-FOG, Parkinson's disease patients with freezing of gait.

74

Wang et al. Topological brain organizations of FOG

observed in PD-FOG.

For nodal parameters, Ne in the left SMA, gyrus rectus, and MCC was negatively correlated with FOG-Q (r=−0.459, $P_{FDR-corr}$=0.019; r=−0.538, $P_{FDR-corr}$=0.008; r=−0.594, $P_{FDR-corr}$=0.004) (*Figure 4B*).

Discussion

With graph theory approaches, we observed impaired structural and relatively reserved functional topological organizations in PD-FOG, providing deeper insights into the neural pathophysiology of this disorder. For structural networks, at the global level, PD-FOG showed increased λ and decreased Eg compared with HCs, and exhibited reduced Eg and Eloc relative to PD-nFOG. At the nodal level, the Ne of the left SMA, gyrus rectus, and MCC was lower in PD-FOG compared with PD-nFOG. In addition, these altered global and nodal properties were significantly correlated with FOG-Q scores in PD-FOG. However, for functional networks, only Eloc was increased in PD-FOG relative to PD-nFOG. No significant structural-functional coupling was identified among the 3 groups.

Whilst previous MRI studies have disclosed associations between PD-FOG and patterns of GM loss, WM tract involvement, and functional alterations, there is little consensus among these studies (23,24,40,41). Such an observation is consistent with the concept that FOG results from the breakdown of an underlying network rather than arising from damage to discrete brain regions (17). Another perspective is to postulate that PD-FOG has a different pathophysiology and circuits, and the key alteration or damage of an individual circuit can imbalance the entire system, whereby a 'weak link' could lead to FOG (6,42). With graph theory approaches, large-scale topological analyses of structural and functional systems enable us to characterize the key 'weak networks and nodes' in the pathophysiological mechanisms of PD-FOG (19). Consistent with previous studies, typical small-world organizations of structural and functional networks were confirmed in our study (24). However, PD-FOG exhibited widely disrupted global and nodal properties in structural networks. Only an increase in the local efficiency of functional networks and even no significant differences in structural-functional coupling were identified in PD-FOG. Meanwhile, the increased local efficiency in PD-FOG was not associated with FOG manifestations, suggesting that it might be a functional compensation secondary to key abnormalities in structural networks and nodes underlying PD-FOG.

Alternatively, it could be a disease characteristic, but not closely related to FOG symptoms. All in all, FOG in PD might be primarily attributable to the network vulnerability established by crucial structural damage.

At the global level, PD-FOG exhibited increased λ but decreased Eg and Eloc of structural networks. Both increase in λ and decrease in Eg reflect a reduction in the ability to transform inter-nodal information over the entire brain, and decreased Eloc represents impaired ability to process information locally (43). Thus, our findings suggested that both impaired global integration and local specialization architectures were critical for the development of FOG in PD. By estimating the diffusivity of water molecules along WM fiber tracts, previous DTI studies revealed FOG-related changes in multiple WM structures, including the PPN, cerebellum, basal ganglia, and frontal and parietal cortices (44-46). Additionally, WM changes focusing on structural connections in PD-FOG were also demonstrated by tractography studies, especially between the PPN and some specific cortical and subcortical regions, such as the cerebellum, thalamus, and frontal cortex (47). With graph theory, Hall *et al.* asserted that a lack of structural integration between some key information processing hubs of the brain contributed to the manifestations of FOG in PD (23). Similarly, our findings demonstrated impaired WM structural global integration and local segregation in PD-FOG. Particularly, reduced global and local efficiency of structural networks in PD-FOG were further negatively correlated with FOG-Q scores, suggesting that the impaired WM structural network might play a key role in the development of FOG in PD.

More specifically, the Ne in the left SMA of the structural system was reduced and correlated with FOG-Q scores in PD-FOG, suggesting that it might be part of the crucial 'weak nodes' in the pathophysiological mechanisms underpinning FOG. The SMA is considered critical for gait control, especially step initiation, as it encodes specific motor sequences and generates an anticipatory postural adjustment (APA) (48). The SMA modulates step initiation by sending information about the postural muscle tone required for context-specific stepping patterns via corticoreticular and reticulospinal tracts (49). Along with the primary motor cortex, the SMA contributes to the output from the corticospinal tract, which elicits voluntary motor commands to step. However, progressive structural damage in the SMA and altered functional connectivity between SMA and other regions known to be involved in step initiation, like the MLR and cerebellar locomotor

regions, have previously been implicated in the pathogenesis of FOG in PD (50-52). Thus, WM structural damage of the SMA might contribute to FOG in PD when an APA is required to initiate gait. Furthermore, noninvasive brain stimulation (NIBS) over the SMA, especially repetitive transcranial magnetic stimulation (rTMS), has emerged as a novel therapeutic approach to alleviate FOG (53,54). Mi *et al.* demonstrated that 10 Hz rTMS over the SMA could improve FOG in PD via normalizing brain connectivity (54). Lench *et al.* found that the SMA in PD-FOG is hyper-connected to the cerebellum, and 1 Hz rTMS could reduce SMA connectivity; however, this was not specific to the locomotor regions (55). Overall, reduced Ne in the left SMA might be involved in the pathophysiological mechanisms of FOG in PD through mediating step initiation during locomotion. The SMA is a promising therapeutic target for NIBS in the treatment of FOG and deserves further investigation.

In addition to the SMA, decreased Ne of the left gyrus rectus and MCC in PD-FOG was also negatively associated with FOG-Q scores, suggesting their important role in PD-FOG pathogenesis. The gyrus rectus is sometimes considered part of the orbitofrontal cortex and is involved in cognitive integration by encoding associations between sensory stimuli of the external world and internal states (56). Proper information integration is essential for normal movement, particularly in cognitively demanding gait tasks. The MCC consists of an anterior part (aMCC) and a posterior part (pMCC). Experimental studies in monkeys have found direct projections to the spinal cord originating from the pMCC (57). The aMCC is functionally coupled to the entire network implementing cognitive motor control through structural connections with the SMA, pre-SMA, premotor cortex, and various parts of the prefrontal cortex (58,59). Thus, structural damage to the left gyrus rectus and MCC might impair gait directly or indirectly by affecting external and internal information integration, abstract cognition translation, and links between cognitive and motor systems. Consistently, there is sufficient evidence to demonstrate structural and functional abnormalities of the left gyrus rectus and MCC in PD-FOG (24,26,60). Taken together, our results suggested that FOG in PD is a complex network disorder. The vulnerable structural networks, especially damaged critical nodes such as the left SMA, gyrus rectus, and MCC, could directly or indirectly contribute to the occurrence of FOG in PD patients.

This study had several limitations. First, limited by rs-fMRI, we were unable to study real-time topological alterations in functional networks and structural-functional coupling before and during FOG onset. However, the structural changes we report are stable and unaffected by the situational presence or absence of FOG events. Second, PD-FOG and PD-nFOG showed higher HAMA and HAMD-24 scores relative to HCs in this study. Clinical studies have disclosed that anxiety and depression are common non-motor features in PD-FOG that crucially contribute to FOG occurrence (61). It is suggested that emotional loading could detract attentional resources in PD-FOG, in turn leading to abrupt gait dysfunction (4,62). Thus, to reduce the potential confounding effects of emotion, we added the HAMA and HAMD-24 scores as covariates in imaging analyses. Third, previous rs-fMRI studies have elucidated other altered brain regions (such as the middle frontal gyrus and cerebellum) (25,26,63) or networks (such as the dorsal attentional network and visual network) (64,65) in PD-FOG by analyzing functional networks. Such inconsistency may be due to differences in included populations, study methods, and statistical thresholds. In our study, Bonferroni correction was applied to explore nodal properties, so our results would have been relatively conservative. However, it also reflected the reliability of our findings. Alternatively, FOG is a network disorder and these alterations in functional networks might be secondary to the breakdown of the structural networks (17). Fourth, altered nodes between PD-FOG and PD-nFOG were detected solely in the left hemisphere, which was not due to lateral heterogeneity of dominant motor symptoms. Although previous studies have shown right cortical and subcortical abnormalities in PD-FOG (47), the role of hemispheric laterality in PD-FOG remains controversial (66). Thus, our findings provide evidence that the pathophysiological mechanisms of PD-FOG are also implicated in the left hemisphere. Finally, the cross-sectional study design limited our ability to confirm how structural and functional brain networks change dynamically as PD develops into PD-FOG. Therefore, future longitudinal studies are needed.

Conclusions

The present study confirms the disrupted structural and relatively reserved functional brain networks in PD-FOG. Topological alterations in structural networks, especially in the left SMA, gyrus rectus, and MCC, contribute to the development of FOG in PD patients.

Footnote

Reporting Checklist: The authors have completed the STROBE reporting checklist. Available at https://qims.amegroups.com/article/view/10.21037/qims-22-351/rc

Conflicts of Interest: All authors have completed the ICMJE uniform disclosure form (available at https://qims.amegroups.com/article/view/10.21037/qims-22-351/coif). The authors have no conflicts of interest to declare.

Ethical Statement: The authors are accountable for all aspects of the work in ensuring that questions related to the accuracy or integrity of any part of the work are appropriately investigated and resolved. The study was conducted in accordance with the Declaration of Helsinki (as revised in 2013). This work was approved by the Ethical Committee of the First Affiliated Hospital of Nanjing Medical University. All participants gave written informed consent.

Open Access Statement: This is an Open Access article distributed in accordance with the Creative Commons Attribution-NonCommercial-NoDerivs 4.0 International License (CC BY-NC-ND 4.0), which permits the non-commercial replication and distribution of the article with the strict proviso that no changes or edits are made and the original work is properly cited (including links to both the formal publication through the relevant DOI and the license). See: https://creativecommons.org/licenses/by-nc-nd/4.0/.

References

1. Giladi N, Nieuwboer A. Understanding and treating freezing of gait in parkinsonism, proposed working definition, and setting the stage. Mov Disord 2008;23 Suppl 2:S423-5.
2. Okuma Y, Silva de Lima AL, Fukae J, Bloem BR, Snijders AH. A prospective study of falls in relation to freezing of gait and response fluctuations in Parkinson's disease. Parkinsonism Relat Disord 2018;46:30-5.
3. Gao C, Liu J, Tan Y, Chen S. Freezing of gait in Parkinson's disease: pathophysiology, risk factors and treatments. Transl Neurodegener 2020;9:12.
4. Bharti K, Suppa A, Tommasin S, Zampogna A, Pietracupa S, Berardelli A, Pantano P. Neuroimaging advances in Parkinson's disease with freezing of gait: A systematic review. Neuroimage Clin 2019;24:102059.
5. Bohnen NI, Kanel P, Zhou Z, Koeppe RA, Frey KA, Dauer WT, Albin RL, Müller MLTM. Cholinergic system changes of falls and freezing of gait in Parkinson's disease. Ann Neurol 2019;85:538-49.
6. Lewis SJ, Shine JM. The Next Step: A Common Neural Mechanism for Freezing of Gait. Neuroscientist 2016;22:72-82.
7. Jha M, Jhunjhunwala K, Sankara BB, Saini J, Kumar JK, Yadav R, Pal PK. Neuropsychological and imaging profile of patients with Parkinson's disease and freezing of gait. Parkinsonism Relat Disord 2015;21:1184-90.
8. Bharti K, Suppa A, Pietracupa S, Upadhyay N, Giannì C, Leodori G, Di Biasio F, Modugno N, Petsas N, Grillea G, Zampogna A, Berardelli A, Pantano P. Abnormal Cerebellar Connectivity Patterns in Patients with Parkinson's Disease and Freezing of Gait. Cerebellum 2019;18:298-308.
9. Guo M, Ren Y, Yu H, Yang H, Cao C, Li Y, Fan G. Alterations in Degree Centrality and Functional Connectivity in Parkinson's Disease Patients With Freezing of Gait: A Resting-State Functional Magnetic Resonance Imaging Study. Front Neurosci 2020;14:582079.
10. Lewis SJ, Barker RA. A pathophysiological model of freezing of gait in Parkinson's disease. Parkinsonism Relat Disord 2009;15:333-8.
11. Nieuwboer A, Giladi N. Characterizing freezing of gait in Parkinson's disease: models of an episodic phenomenon. Mov Disord 2013;28:1509-19.
12. Maidan I, Jacob Y, Giladi N, Hausdorff JM, Mirelman A. Altered organization of the dorsal attention network is associated with freezing of gait in Parkinson's disease. Parkinsonism Relat Disord 2019;63:77-82.
13. Bharti K, Suppa A, Pietracupa S, Upadhyay N, Giannì C, Leodori G, Di Biasio F, Modugno N, Petsas N, Grillea G, Zampogna A, Berardelli A, Pantano P. Aberrant functional connectivity in patients with Parkinson's disease and freezing of gait: a within- and between-network analysis. Brain Imaging Behav 2020;14:1543-54.
14. Li Y, Ruan X, Li E, Zhang G, Liu Y, Du Y, Wang Z, Yu S, Yang R, Li M, Wei X. Aberrant Advanced Cognitive and Attention-Related Brain Networks in Parkinson's Disease

with Freezing of Gait. Neural Plast 2020;2020:8891458.

15. Gilat M, Ehgoetz Martens KA, Miranda-Domínguez O, Arpan I, Shine JM, Mancini M, Fair DA, Lewis SJG, Horak FB. Dysfunctional Limbic Circuitry Underlying Freezing of Gait in Parkinson's Disease. Neuroscience 2018;374:119-32.

16. Ehgoetz Martens KA, Hall JM, Georgiades MJ, Gilat M, Walton CC, Matar E, Lewis SJG, Shine JM. The functional network signature of heterogeneity in freezing of gait. Brain 2018;141:1145-60.

17. Weiss D, Schoellmann A, Fox MD, Bohnen NI, Factor SA, Nieuwboer A, Hallett M, Lewis SJG. Freezing of gait: understanding the complexity of an enigmatic phenomenon. Brain 2020;143:14-30.

18. Pozzi NG, Canessa A, Palmisano C, Brumberg J, Steigerwald F, Reich MM, Minafra B, Pacchetti C, Pezzoli G, Volkmann J, Isaias IU. Freezing of gait in Parkinson's disease reflects a sudden derangement of locomotor network dynamics. Brain 2019;142:2037-50.

19. Bullmore E, Sporns O. Complex brain networks: graph theoretical analysis of structural and functional systems. Nat Rev Neurosci 2009;10:186-98.

20. Cao Y, Zhan Y, Du M, Zhao G, Liu Z, Zhou F, He L. Disruption of human brain connectivity networks in patients with cervical spondylotic myelopathy. Quant Imaging Med Surg 2021;11:3418-30.

21. Latora V, Marchiori M. Efficient behavior of small-world networks. Phys Rev Lett 2001;87:198701.

22. Wang L, Wang M, Si Q, Yuan Y, Ma K, Gan C, Zhang K. Altered brain structural topological properties in Parkinson's disease with levodopa-induced dyskinesias. Parkinsonism Relat Disord 2019;67:36-41.

23. Hall JM, Shine JM, Ehgoetz Martens KA, Gilat M, Broadhouse KM, Szeto JYY, Walton CC, Moustafa AA, Lewis SJG. Alterations in white matter network topology contribute to freezing of gait in Parkinson's disease. J Neurol 2018;265:1353-64.

24. Ruan X, Li Y, Li E, Xie F, Zhang G, Luo Z, Du Y, Jiang X, Li M, Wei X. Impaired Topographical Organization of Functional Brain Networks in Parkinson's Disease Patients With Freezing of Gait. Front Aging Neurosci 2020;12:580564.

25. Li N, Suo X, Zhang J, Lei D, Wang L, Li J, Peng J, Duan L, Gong Q, Peng R. Disrupted functional brain network topology in Parkinson's disease patients with freezing of gait. Neurosci Lett 2021;759:135970.

26. Li N, Lei D, Peng J, Suo X, Li J, Duan L, Chen C, Gong Q, Peng R. Brain network topology and future development

of freezing of gait in Parkinson's disease: a longitudinal study. J Neurol 2022;269:2503-12.

27. Wang YF, Gu P, Zhang J, Qi R, de Veer M, Zheng G, Xu Q, Liu Y, Lu GM, Zhang LJ. Deteriorated functional and structural brain networks and normally appearing functional-structural coupling in diabetic kidney disease: a graph theory-based magnetic resonance imaging study. Eur Radiol 2019;29:5577-89.

28. Goetz CG, Tilley BC, Shaftman SR, Stebbins GT, Fahn S, Martinez-Martin P, et al. Movement Disorder Society-sponsored revision of the Unified Parkinson's Disease Rating Scale (MDS-UPDRS): scale presentation and clinimetric testing results. Mov Disord 2008;23:2129-70.

29. Crum RM, Anthony JC, Bassett SS, Folstein MF. Population-based norms for the Mini-Mental State Examination by age and educational level. JAMA 1993;269:2386-91.

30. Giladi N, Shabtai H, Simon ES, Biran S, Tal J, Korczyn AD. Construction of freezing of gait questionnaire for patients with Parkinsonism. Parkinsonism Relat Disord 2000;6:165-70.

31. Goetz CG, Poewe W, Rascol O, Sampaio C, Stebbins GT, Counsell C, Giladi N, Holloway RG, Moore CG, Wenning GK, Yahr MD, Seidl L; Movement Disorder Society Task Force on Rating Scales for Parkinson's Disease. Movement Disorder Society Task Force report on the Hoehn and Yahr staging scale: status and recommendations. Mov Disord 2004;19:1020-8.

32. Movement Disorder Society Task Force on Rating Scales for Parkinson's Disease. The Unified Parkinson's Disease Rating Scale (UPDRS): status and recommendations. Mov Disord 2003;18:738-50.

33. Kegelmeyer DA, Kloos AD, Thomas KM, Kostyk SK. Reliability and validity of the Tinetti Mobility Test for individuals with Parkinson disease. Phys Ther 2007;87:1369-78.

34. Podsiadlo D, Richardson S. The timed "Up & Go": a test of basic functional mobility for frail elderly persons. J Am Geriatr Soc 1991;39:142-8.

35. HAMILTON M. The assessment of anxiety states by rating. Br J Med Psychol 1959;32:50-5.

36. HAMILTON M. A rating scale for depression. J Neurol Neurosurg Psychiatry 1960;23:56-62.

37. Dubois B, Slachevsky A, Litvan I, Pillon B. The FAB: a Frontal Assessment Battery at bedside. Neurology 2000;55:1621-6.

38. Tomlinson CL, Stowe R, Patel S, Rick C, Gray R, Clarke CE. Systematic review of levodopa dose

78

Wang et al. Topological brain organizations of FOG

equivalency reporting in Parkinson's disease. Mov Disord 2010;25:2649-53.

39. Zhang J, Wang J, Wu Q, Kuang W, Huang X, He Y, Gong Q. Disrupted brain connectivity networks in drug-naive, first-episode major depressive disorder. Biol Psychiatry 2011;70:334-42.

40. Tessitore A, Amboni M, Cirillo G, Corbo D, Picillo M, Russo A, Vitale C, Santangelo G, Erro R, Cirillo M, Esposito F, Barone P, Tedeschi G. Regional gray matter atrophy in patients with Parkinson disease and freezing of gait. AJNR Am J Neuroradiol 2012;33:1804-9.

41. Pietracupa S, Suppa A, Upadhyay N, Giannì C, Grillea G, Leodori G, Modugno N, Di Biasio F, Zampogna A, Colonnese C, Berardelli A, Pantano P. Freezing of gait in Parkinson's disease: gray and white matter abnormalities. J Neurol 2018;265:52-62.

42. Fasano A, Herman T, Tessitore A, Strafella AP, Bohnen NI. Neuroimaging of Freezing of Gait. J Parkinsons Dis 2015;5:241-54.

43. Rubinov M, Sporns O. Complex network measures of brain connectivity: uses and interpretations. Neuroimage 2010;52:1059-69.

44. Jin C, Qi S, Teng Y, Li C, Yao Y, Ruan X, Wei X. Integrating Structural and Functional Interhemispheric Brain Connectivity of Gait Freezing in Parkinson's Disease. Front Neurol 2021;12:609866.

45. Vercruysse S, Leunissen I, Vervoort G, Vandenberghe W, Swinnen S, Nieuwboer A. Microstructural changes in white matter associated with freezing of gait in Parkinson's disease. Mov Disord 2015;30:567-76.

46. Wang M, Jiang S, Yuan Y, Zhang L, Ding J, Wang J, Zhang J, Zhang K, Wang J. Alterations of functional and structural connectivity of freezing of gait in Parkinson's disease. J Neurol 2016;263:1583-92.

47. Fling BW, Cohen RG, Mancini M, Nutt JG, Fair DA, Horak FB. Asymmetric pedunculopontine network connectivity in parkinsonian patients with freezing of gait. Brain 2013;136:2405-18.

48. Massion J. Movement, posture and equilibrium: interaction and coordination. Prog Neurobiol 1992;38:35-56.

49. Takakusaki K. Functional Neuroanatomy for Posture and Gait Control. J Mov Disord 2017;10:1-17.

50. Youn J, Cho JW, Lee WY, Kim GM, Kim ST, Kim HT. Diffusion tensor imaging of freezing of gait in patients with white matter changes. Mov Disord 2012;27:760-4.

51. Fling BW, Cohen RG, Mancini M, Carpenter SD, Fair DA, Nutt JG, Horak FB. Functional reorganization of the locomotor network in Parkinson patients with freezing of

gait. PLoS One 2014;9:e100291.

52. de Lima-Pardini AC, Coelho DB, Nucci MP, Boffino CC, Batista AX, de Azevedo Neto RM, Silva-Batista C, Barbosa ER, Cohen RG, Horak FB, Teixeira LA, Amaro E Jr. Brain networks associated with anticipatory postural adjustments in Parkinson's disease patients with freezing of gait. Neuroimage Clin 2020;28:102461.

53. Kim SJ, Paeng SH, Kang SY. Stimulation in Supplementary Motor Area Versus Motor Cortex for Freezing of Gait in Parkinson's Disease. J Clin Neurol 2018;14:320-6.

54. Mi TM, Garg S, Ba F, Liu AP, Liang PP, Gao LL, Jia Q, Xu EH, Li KC, Chan P, McKeown MJ. Repetitive transcranial magnetic stimulation improves Parkinson's freezing of gait via normalizing brain connectivity. NPJ Parkinsons Dis 2020;6:16.

55. Lench DH, DeVries W, Kearney-Ramos TE, Chesnutt A, Monsch ED, Embry AE, Doolittle JD, Kautz SA, Hanlon CA, Revuelta GJ. Paired inhibitory stimulation and gait training modulates supplemental motor area connectivity in freezing of gait. Parkinsonism Relat Disord 2021;88:28-33.

56. Rudebeck PH, Rich EL. Orbitofrontal cortex. Curr Biol 2018;28:R1083-8.

57. Dum RP, Strick PL. The origin of corticospinal projections from the premotor areas in the frontal lobe. J Neurosci 1991;11:667-89.

58. Morecraft RJ, Stilwell-Morecraft KS, Cipolloni PB, Ge J, McNeal DW, Pandya DN. Cytoarchitecture and cortical connections of the anterior cingulate and adjacent somatomotor fields in the rhesus monkey. Brain Res Bull 2012;87:457-97.

59. Hoffstaedter F, Grefkes C, Caspers S, Roski C, Palomero-Gallagher N, Laird AR, Fox PT, Eickhoff SB. The role of anterior midcingulate cortex in cognitive motor control: evidence from functional connectivity analyses. Hum Brain Mapp 2014;35:2741-53.

60. Vastik M, Hok P, Valosek J, Hlustik P, Mensikova K, Kanovsky P. Freezing of gait is associated with cortical thinning in mesial frontal cortex. Biomed Pap Med Fac Univ Palacky Olomouc Czech Repub 2017;161:389-96.

61. Ehgoetz Martens KA, Ellard CG, Almeida QJ. Does anxiety cause freezing of gait in Parkinson's disease? PLoS One 2014;9:e106561.

62. Taylor NL, Wainstein G, Quek D, Lewis SJG, Shine JM, Ehgoetz Martens KA. The Contribution of Noradrenergic Activity to Anxiety-Induced Freezing of Gait. Mov Disord 2022;37:1432-43.

63. Jin C, Qi S, Teng Y, Li C, Yao Y, Ruan X, Wei X. Altered

Degree Centrality of Brain Networks in Parkinson's Disease With Freezing of Gait: A Resting-State Functional MRI Study. Front Neurol 2021;12:743135.

64. Yu Q, Li Q, Fang W, Wang Y, Zhu Y, Wang J, Shen Y, Han Y, Zou D, Cheng O. Disorganized resting-state functional connectivity between the dorsal attention network and intrinsic networks in Parkinson's disease with freezing of gait. Eur J Neurosci 2021;54:6633-45.

65. Steidel K, Ruppert MC, Palaghia I, Greuel A, Tahmasian M, Maier F, Hammes J, van Eimeren T, Timmermann L, Tittgemeyer M, Drzezga A, Pedrosa D, Eggers C. Dopaminergic pathways and resting-state functional connectivity in Parkinson's disease with freezing of gait. Neuroimage Clin 2021;32:102899.

66. Pieruccini-Faria F, Ehgoetz Martens KA, Silveira CR, Jones JA, Almeida QJ. Side of basal ganglia degeneration influences freezing of gait in Parkinson's disease. Behav Neurosci 2015;129:214-8.

Appendix 1 Supplementary methods

Imaging parameters

Whole-brain T1-weighted anatomical images were acquired using the following volumetric 3D magnetization-prepared rapid gradient-echo (MP-RAGE) sequence. Scan parameters were as follows: repetition time (TR) = 1900 ms, echo time (TE) = 2.95 ms, flip angle = 9°, slice thickness = 1 mm, slices = 160, field of view (FOV) = 230 × 230 mm^2, matrix size = 256 × 256 and voxel size = 1 × 1 × 1 mm^3.

Diffusion tensor imaging (DTI) data were obtained using spin echo planar imaging sequence. Parameters were as follows: TR = 9800 ms, TE = 95 ms, FOV = 256 × 256 mm^2, number of excitations (NEX) = 1, matrix = 128 × 128, slice thickness = 2 mm and slice gap = 0 mm. Diffusion gradients were applied in 30 non-collinear directions with a b factor of 1000 s/mm^2 after an acquisition without diffusion weighting (b = 0 s/mm^2) for reference.

Besides, whole brain resting-state functional MR imaging (rs-fMRI) data were gained with an echo-planar imaging (EPI) sequence. During scanning, all participants were instructed to stay awake, keep their head still, relax with their eyes closed, and not think of anything in particular. Scan parameters were as follows: TR = 2000 ms, TE = 21 ms, flip angle = 90°, FOV = 256 × 256 mm^2, in-plane matrix = 64 × 64, slice thickness = 3 mm, number of slices = 35, no slice gap, voxel size = 3 × 3 × 3 mm^3 and total volumes = 240.

MRI data preprocessing

DTI data preprocessing steps included brain extraction, realignment, eddy current and motion artifact correction, fractional anisotropy (FA) calculation, and diffusion tensor tractography. All these steps were performed using the PANDA toolbox based on FMRIB Software Library. Deterministic fiber tracking was applied to construct white matter (WM) structural brain networks. The fiber tracking was performed using Continuous Tracking algorithm. The FA threshold was set to 0.2, and the turning angle threshold was set to 45° for the fiber assignment. The quality controls and analyses of magnetic resonance images were performed by an experienced imaging scientist (Min Wang, with 10 years of experience in MRI data analysis).

The preprocessing of rs-fMRI data was performed using the Data Processing Assistant for rs-fMRI (DPARSF) based on Statistical Parametric Mapping (SPM). Removed the first 10 time points to reduce transient signal changes caused by unstable magnetic field and to permit subjects to be accustomed to the scanning circumstance. Afterwards, preprocessing included standard slice timing, head motion correction, realignment, spatial normalization by diffeomorphic anatomical registration through exponentiated lie algebra (DARTEL; voxel size [3, 3, 3]), smoothing at 6 mm full-width half maximum (FWHM), temporal band-pass filtering (0.01-0.08 Hz) and nuisance signals regression (including six head motion parameters, average WM, cerebrospinal fluid and global signals). Finally, individuals with more than 2.0 mm or 2-degree cumulative translation or rotation head motion were excluded from our study.

Construction of brain networks

To construct WM structural networks, each brain was parcellated into 116 regions of interest (ROIs) using Anatomical Automatic Labeling (AAL) atlas (including the cerebellum), which were defined as 116 nodes. The parcellation process was performed in the native space. Actually, T1-weighted images of each participant were firstly registered with their corresponding b = 0 image with an affine transformation. Afterwards, the individual transformed T1-weighted images were registered to the ICBM152 T1 template (Montreal Neurological Institute, Montreal, Canada) by a non-linear transformation. Finally, the inversed transformation parameter of each individual was applied to the AAL atlas to generate corresponding AAL regions in individual space. Each AAL region was considered as a node, and interconnections between brain regions (interconnected WM fiber numbers in this study) were considered as the edges of the structural network. Finally, a symmetrically structural connectivity matrix (116 × 116) for each individual was obtained.

Functional networks were constructed using the GRETNA toolbox. Same as before, AAL116 atlas was chosen as the parcellation scheme. Then, A 116 × 116 temporal correlation matrix was assembled by computing Pearson's correlation coefficient between the residual time series of each pair of the 116 nodes for each participant. For each ROI, the mean

time series were obtained by averaging the fMRI time courses over each ROI. The values of the interregional correlation coefficients were taken as the weights of the edges. Finally, we performed the Fisher's r-to-z transformation to improve the normality of the correlation.

Structural-functional coupling analysis

First, all non-zero connectivities of the structural networks were selected. Second, these connectivity values were rescaled to a Gaussian distribution. Finally, the corresponding connectivities of the functional networks were also extracted and correlated with the structural counterparts selected forehead. And this resulted in a single structural-functional coupling value for each subject (67,68).

References

67. Hagmann P, Sporns O, Madan N, Cammoun L, Pienaar R, Wedeen VJ, Meuli R, Thiran JP, Grant PE. White matter maturation reshapes structural connectivity in the late developing human brain. Proc Natl Acad Sci U S A 2010;107:19067-72.
68. Honey CJ, Sporns O, Cammoun L, Gigandet X, Thiran JP, Meuli R, Hagmann P. Predicting human resting-state functional connectivity from structural connectivity. Proc Natl Acad Sci U S A 2009;106:2035-40.